Research Square

Preprints are preliminary reports that have not undergone peer review.
They should not be considered conclusive, used to inform clinical practice,
or referenced by the media as validated information.

Radiation-Sparing Intravenous DSA and Augmented Reality Navigation in Pediatric Neurosurgery: A Quantitative Analysis of Perioperative Effective Dose and Workflow

Chih-Wei Huang
Chung Shan Medical University
Chiu-Chun Chen
Taichung Veterans General Hospital
Kai-Chen Chung
Taichung Veterans General Hospital
Pei-Ying Tseng
Asia University
Che-Hao Lin
Taichung Veterans General Hospital
Bai-Shuan Liu
Central Taiwan University of Science and Technology
Yuang-Seng Tsuei
astrocytoma2001@yahoo.com.tw

National Chung Hsing University
Shun-Fa Yang
Chung Shan Medical University

Research Article

Keywords: arteriovenous malformations, augmented reality, digital subtraction angiography

Posted Date: May 11th, 2026

DOI: https://doi.org/10.21203/rs.3.rs-9167196/v1

License: This work is licensed under a Creative Commons Attribution 4.0 International License.
Read Full License

Additional Declarations: No competing interests reported.

Abstract

Conventional intra-arterial angiography remains the standard for brain arteriovenous malformation surgery but carries inherent risks of arterial complications and significant radiation exposure in children. This study evaluates the feasibility and radiation-sparing benefits of an intravenous angiography protocol integrated with augmented reality navigation for pediatric brain malformation resection. We retrospectively analyzed three pediatric cases where Cases 1 and 2 utilized a tailored intravenous digital subtraction angiography protocol for augmented reality navigation, while Case 3 served as a comparative control using conventional perioperative intra-arterial angiography. The optimized intravenous protocol yielded a standardized effective dose of 0.83 mSv per session. In Case 1, the total effective dose for two intravenous sessions, covering both preoperative mapping and postoperative confirmation, was only 1.92 mSv. In contrast, the perioperative intra-arterial angiography in Case 3 resulted in a total dose of 12.70 mSv, representing an 85% reduction in radiation exposure. Furthermore, the intravenous workflow optimized operative time by eliminating invasive arterial maneuvers, and navigation accuracy was maintained even in the presence of severe intraoperative brain shift through manual realignment. This protocol provides a robust and radiation-efficient alternative for pediatric surgery, effectively implementing the principle of keeping radiation exposure as low as reasonably achievable.

INTRODUCTION

Arteriovenous malformations (AVMs) are complex vascular anomalies characterized by direct connections between the arteries and veins without intermediary capillary networks, thereby disrupting blood circulation and oxygen transport.[1] Brain AVMs (bAVMs) can jeopardize the cerebral steal phenomenon, seizures, headache, aneurysm or venous stenosis formation, and intracerebral hemorrhage,[2] and are the leading cause of pediatric intracerebral hemorrhage, accounting for up to 55% of cases.[3] The annual hemorrhage risk due to pediatric bAVM ranges from 2%–10%,[4] which is higher than that in the adult population (1%–3%).[5] In one study, distribution in the posterior fossa or basal ganglion, which exhibits a greater rupture risk, was more frequently noted in pediatric AVMs than in adult AVMs.[6] The mortality rate of bAVM in children can be as high as 21%.[2] Therefore, this should be proactively addressed.

Surgical resection remains the primary treatment option for bAVMs with low Spetzler–Martin grades[7]. First, surgical resection leads to an instant cure and a higher obliteration rate than pure radiosurgery or endovascular intervention.[4] Otherwise, non-surgical treatment is required, which is a long-term process for children and their guardians. Second, radiosurgery increases radiation exposure. Third, endovascular intervention is less feasible for children because of the limited sizes of catheters, wires, and coils. However, surgical resection of pediatric bAVM is linked to several challenges. Surgeons should consider the balance between complete AVM resection and preservation of neurological function, especially when the lesion is in a crucial neurovascular region. Additionally, pediatric hemodynamic fragility and

variability significantly increase perioperative risks, as children have less total blood volume compared to adults. The body surface area of a child is greater than that of an adult; therefore, children are more susceptible to fluid loss and hypothermia induced by long surgery durations[8]; in particular, hypothermia can induce coagulopathy and suppress cardiorespiration. Furthermore, hypotension is a late sign of hemorrhagic shock in children, which may reduce the ability to assess blood loss.[9]

Consequently, comprehensive perioperative planning is required for pediatric AVM resections. Various imaging technologies have been introduced to deconstruct lesions and aid surgery, including intra-arterial digital subtraction angiography (IA-DSA), multidetector computed tomography (MDCT) angiography-based navigation, and augmented reality (AR). However, current imaging protocols documented in literature inevitably result in substantial radiation exposure and increased procedural risks, particularly in pediatric populations.

Given the existing challenges of pediatric neurointervention—such as fragile vasculature, limited training resources, prolonged interventionalist standby, and high procedural costs—we extended our previously validated adult IV-DSA method to pediatric patients. Therefore, we adapted and implemented our established intravenous digital subtraction angiography (IV-DSA) technique, combined with AR navigation, for pediatric bAVM surgery, aiming to enhance surgical precision, reduce invasiveness, and minimize radiation exposure. This protocol provides an efficient and smooth surgical process with greater precision and adjustability but lower invasiveness and radiation exposure.

METHODS

This study was conducted in a hybrid operating room using an IV-DSA and AR-guided protocol for pediatric bAVM resection. The surgical workflow was adapted from previous protocols[10], with modifications in contrast volume, injection rate, and timing tailored to pediatric physiology.

Source imaging was acquired using an iFlow-tailored IV-DSA protocol with a biplane angiography system (ARTIS icono, Siemens Healthineers, Germany).

A preliminary test injection was administered via a central venous catheter (CVC) at a flow rate of 3.5 mL/s, using a total contrast volume of 1 mL/kg, followed by a saline flush of double that volume. Optimal scan delay was determined using iFlow software (syngo, Siemens), which analyzes contrast kinetics and generates a color-coded intensity map[10]. To minimize cortical shift during craniotomy, patients were positioned using a radiolucent head holder. After dural opening, a formal 3D DSA scan was performed using 1–1.5 mL/kg of contrast at an injection rate of 2.5–3.5 mL/s. The angioarchitecture, including feeding arteries, draining veins, AVM nidus, and cortical surface landmarks, was segmented using SmartBrush (Brainlab, IL, USA). These labels were then coregistered with the navigation system and fused with intraoperative microscopy using the KINEVO surgical microscope (ZEISS, Germany).

During resection, primary arterial feeders were identified and occluded with surgical clips applied as proximally to the nidus as feasible. The AVM nidus was subsequently removed under continuous AR

guidance, allowing real-time orientation between the anatomical structures and projected vascular models.

RESULTS

We present two representative pediatric cases to demonstrate the applicability of IV-DSA AR-guided bAVM surgery in both elective and urgent settings. Case 1 involved a scheduled procedure for an unruptured lesion, while Case 2 required second-stage surgery for a previously ruptured AVM with significant cerebral edema. Detailed perioperative information is summarized in Table 1. We also illustrated Case 3, who received resection of a ruptured AVM under IA-DSA AR guided-guided surgery as comparison.

Table 1
Summary of two representative cases reported herein

Body weight	**Case 1**	**Case 2**
	30 kg	**12 kg**
Presentation	Unruptured, absence of seizures	Intracerebral hemorrhage with brain edema
AVM, SM grade, location	SM = 1, left frontal lobe	SM = 1, left parietal lobe
IV route	Right neck CVC	Left neck CVC
Protocol of the test round	10 mL contrast (3.5 mL/s), bolus with 50 mL saline	4 cc contrast (2.5 mL/s), bolus with 16 mL saline
Timing of the test round	Supine, before positioning	Supine, before positioning
Delayed time	9 s	8 s
3D DSA, 4 s	3D DSA, 4 s	3D DSA, 4 s
3D DSA protocol	30 mL contrast (3.5 mL/s), bolus with 30 mL saline	10 mL contrast (2.5 mL/s), bolus with 10 mL saline
Fixation	3-pin radiolucent head holder	Horseshoe radiolucent head supporter
Timing of 3D DSA	After dura opening	Before dura opening
Image quality for navigation	Good	Fair (peripheral, small-sized vessel, and brain edema)

AVM, arteriovenous malformation; CVC, central venous catheter; DSA, digital subtraction angiography; SM, Spetzler–Martin.

Case 1

A school-aged child with an unruptured left frontal AVM (Spetzler–Martin grade I) underwent surgery with intraoperative IV-DSA. Imaging identified two major feeders from the left anterior cerebral artery, several minor feeders from the left middle cerebral artery, and a single superficial draining vein (Fig. 1). Total blood loss was approximately 100 mL, and operative time was 6.5 hours, including IV-DSA setup. The effective radiation dose was 1.92 mSv. The patient had no postoperative neurological deficits and was discharged on postoperative day 6.

Case 2

A preschool-aged child with a ruptured left parietal–occipital AVM and signs of increased intracranial pressure (GCS E3V1M5) underwent craniectomy and hematoma evacuation at an outside facility, followed by transfer. On postoperative day 8, a second-stage resection was performed. Due to anticipated brain shift from edema, IV-DSA was performed pre-craniotomy. Imaging revealed two major feeders from the left middle cerebral artery and one superficial draining vein. Brain swelling induced AR overlay deviation, requiring manual adjustment to realign with cortical structures. Resection and cranioplasty were completed within 4 hours (Fig. 2). The effective radiation dose was 7.91 mSv. The patient recovered full consciousness and limb strength by postoperative day 2 and was discharged on day 8.

Case 3

A school-aged child with a ruptured right frontal-parietal AVM and left lower limb weakness (muscle power grade 4) underwent craniotomy with intraoperative IA-DSA. Imaging revealed main feeding arteries from right anterior cerebral artery. Brain swelling also led to AR overlay deviation, which was overcame by manual readjustment. Operative time was 8 hours, including IA-DSA operation. The effective radiation dose was 12.70 mSv. The patient recovered limb strength and was discharged on day 11.

Calculation of the effective IV-DSA dose

IV-DSA consisted of three steps: (i) the iFlow method was used as a test round; (ii) the required time window was calculated; and (iii) a time-specific 3D scan was performed. The effective radiation dose was calculated as:

Effective radiation dose (mSV) = Dose area product (DAP) ($\mu Gy \cdot m^2$) × 0.055 mSv/Gy·cm²

The conversion factor was 0.055 mSv/Gy·cm^2 for cerebral angiography based on previous studies[11,12].

In our setting, single-plane IV-DSA (4 frames/s) yielded DAP values of approximately 600–700μGy·m². A representative value of 650 μGy·m² was used for standardization. For 3D DSA (68 frames/s), DAP was approximately 850 μGy·m².

The effective dose was calculated as follows:

Test injection (using single plane): 650 μGy·m² × 0.055 mSv/Gy·cm² = 0.36 mSv

3D DSA acquisition: 850 μGy·m² × 0.055 mSv/Gy·cm² = 0.47 mSv

Total IV-DSA per session: 0.36 + 0.47 = 0.83 mSv

For cases in which only a preoperative IV-DSA was performed, the effective dose remained as low as 0.83 mSv, highlighting its radiation-sparing advantage.

Comparison of radiation exposure between imaging protocols

Table 2 summarizes the effective radiation doses associated with different imaging modalities across clinical settings. Preoperative IV-DSA involves both a test and formal round, resulting in a total dose of approximately 0.83 mSv. In contrast, intraoperative or postoperative evaluations typically require only a repeat 3D scan (0.47 mSv) to assess residual nidus.

Table 2
Effective radiation doses of various imaging tools at different times

Effective radiation dose of various imaging tools at different times					
Imaging tools	CTA	IA-DSA	IV-DSA		
Timing	(lowest dose)	(lowest dose)	Single plane		
			Total	iFlow	3D DSA
Preoperative	3.3 mSv	2.8 mSv	0.83 mSv	0.36 mSv	0.47 mSv
Intraoperative	3.3 mSv	2.8 mSv	0.47 mSv	0	0.47 mSv
Postoperative	3.3 mSv	2.8 mSv	0.47 mSv	0	0.47 mSv
Accumulation effective radiation dose					
Imaging tools	CTA	IA-DSA	Single plane		
Number of times	(lowest dose)	(lowest dose)		IV-DSA/CTA	IV-DSA/IA-DSA
1	3.3 mSv	2.8 mSv	0.83 mSv	25.2%	29.6%
2	6.6 mSv	5.6 mSv	1.30 mSv	19.7%	23.2%
3	9.9 mSv	8.4 mSv	1.77 mSv	17.9%	21.1%

CTA, computed tomography angiography; IA-DSA, intra-arterial digital subtraction angiography; IV-DSA, intravenous digital subtraction angiography.

Contrastingly, the radiation doses of computed tomography angiography (CTA) and IV-DSA are fixed regardless of the preoperative, intraoperative, or postoperative settings. The effective dose of each type of MDCT angiography ranged approximately from 3.3–7 mSv in the published literature and data from our institute,[12–14] whereas the value of IA-DSA was between 2.8 and 14.4 mSv.[12,15] In Case 3, the effective dose of IA-DSA was 12.70 mSv. Generally, the effective dose of IV-DSA is lower than that of MDCT angiography or IA-DSA.

To quantify this benefit, we compared cumulative IV-DSA exposure to CTA and IA-DSA using the lowest reported values: 3.3 mSv for CTA and 2.8 mSv for IA-DSA. After one full IV-DSA session (0.83 mSv), the relative dose ratios were 25.2% (IV-DSA/CTA) and 29.6% (IV-DSA/IA-DSA). With repeated imaging—such as preoperative mapping, intraoperative confirmation, and postoperative surveillance—, the cumulated IV-DSA dose reached only 1.77 mSv, equivalent to only 17.9% and 21.1% of accumulative CTA and IA-DSA doses, respectively. These findings emphasize the radiation-sparing advantage of IV-DSA in pediatric AVM management. This trend is visualized in Fig. 3, which compares the cumulative effective doses of each modality across 1–3 sessions. The graph clearly demonstrates that IV-DSA maintains a substantial dose advantage over CTA and IA-DSA at every time point.

DISCUSSION

Protocol Innovation and Pediatric Adaptation

Few studies have proposed standardized IV-DSA protocols, particularly in children. Prior adult reports (e.g., Spetzler–Martin grade I parietal AVM[10]) mentioned 15 mL (test) and 50 mL (formal) contrast injections at 5 mL/s, with a 19-second delay. However, critical imaging parameters such as timing methods or IV route were often unreported[16].

To adapt for pediatric physiology, we referenced Thust et al.[17], which recommended 2.5–4.0 mL/s and 1–2 mL/kg in children. In our cases, we used 1 mL/kg at 3.5 mL/s for unruptured AVM, and 0.8 mL/kg at 2.5 mL/s for a 4-year-old with IICP. Despite image distortion from edema and peripheral vessels, vessel orientation remained clinically useful.

The iFlow-guided test round and enhancement curve allowed individualized scan timing, improving upon pediatric CTA, which relies on aortic triggers often inaccurate due to cardiac variability. In Thust's cohort[17], one-third of CTA images were suboptimal. Our results show IV-DSA with iFlow provides more precise and pediatric-tailored imaging.

Radiation Safety and Pediatric Considerations

Radiation exposure in pediatric patients is not only linked to carcinogenesis[18] but also to neurocognitive impairment. According to the International Commission on Radiological Protection, 1 Sv of radiation carries an estimated cancer risk of 5.5% in the general population, and a heritable risk of 0.2% per Sv [19]. Childhood studies have shown that cumulative exposures exceeding 24 Gy in children under 3 years, and

36 Gy in those under 6 years, are associated with measurable reductions in IQ [20]. These statistics highlight the necessity of minimizing dose, particularly in children who may undergo multiple imaging sessions.

In this study, our IV-DSA AR-guided protocol demonstrated a substantial reduction in radiation exposure compared to conventional CTA and IA-DSA. A full IV-DSA session delivered only 0.83 mSv—approximately 25.2% of CTA and 29.6% of IA-DSA dose equivalents. With three imaging sessions, the cumulative IV-DSA dose remained below 2 mSv, representing 17.9% and 21.1% of CTA and IA-DSA, respectively. These findings, supported visually by Fig. 3, reinforce the dose-sparing potential of IV-DSA for pediatric cerebrovascular evaluation.

While current guidelines emphasize radiation limits in adults, children are disproportionately vulnerable due to developing tissues and higher effective dose per organ mass. The cumulative effect is more pronounced when imaging is repeated over years for follow-up or residual lesion surveillance. In this context, even small reductions per imaging session compound into clinically meaningful benefits for pediatric patients. Furthermore, radiation-induced vascular changes, particularly in developing cerebral vasculature, may have long-term consequences not fully documented in current literature. These risks underscore the necessity of reducing unnecessary exposure in pediatric neurovascular procedures.

Clinical Feasibility and Technical Adaptation of IV-DSA

DSA remains a cornerstone in AVM surgical planning. However, conventional intra-arterial DSA (IA-DSA)—especially via the transfemoral route—is associated with procedural risks including groin hematoma, ischemic or hemorrhagic stroke, vasospasm, and arterial dissection. The complication rate of transfemoral DSA in pediatric groups ranges from 3.3% to 4.8%[21–23], whereas the overall complication rate in adult groups ranges from 0.5% to 2.6%[24,25].

Transradial DSA, though preferred in adults for its reduced groin-related complications, is generally contraindicated in young children. Alehaideb et al. reported that the average radial artery diameter in children under 12 years is less than 2 mm[26], below the minimum threshold for safe cannulation. Furthermore, pediatric patients show higher rates of radial artery spasm (23%), stenosis (7.7%), thrombotic occlusion (3.8%), and hematoma (7.7%) compared to adults, whose overall complication risk is around 1.8%[27,28].

Given these anatomical and physiological constraints, IV-DSA via CVC—routinely placed for pediatric anesthesia—offers a safer, less invasive, and more practical alternative. The technique allows angiographic acquisition from multiple vascular territories in a single session without repositioning the catheter and eliminates the need for intra-arterial navigation through tortuous vasculature. This minimizes vascular trauma and shortens procedure time. Furthermore, unlike IA-DSA which mandates a supine position, IV-DSA permits flexible patient positioning. This is particularly beneficial in pediatric bAVM surgeries involving posterior fossa lesions, where prone or lateral positioning is often required. In

such cases, arterial catheter fixation can be difficult and time-consuming, further highlighting the procedural convenience of IV-DSA.

While Table 2 establishes an optimized baseline where the minimum effective dose (ED) for IA-DSA is 2.8 mSv, our clinical cases illustrate a substantial divergence between idealized benchmarks and real-world neurosurgical practice. In Case 3, the IA-DSA required a total dose of 12.70 mSv—more than 4.5 times its theoretical minimum—due to the inherent complexities of intraoperative arterial navigation and repeated roadmapping.

Conversely, although the ED in Case 1 (1.92 mSv) and Case 2 (7.91 mSv) exceeded the idealized IV-DSA benchmark of 0.83 mSv, these values remained consistently lower than the corresponding IA-DSA requirements. This disparity underscores the superior "dose predictability" of our IV-DSA protocol. In pediatric patients, where anatomical fragility often complicates intra-arterial access, the IV-DSA approach ensures that even in urgent scenarios with significant brain shift (as demonstrated in Case 2), radiation exposure remains managed and significantly lower than the cumulative risks associated with traditional intra-arterial maneuvers.

Importantly, this technique is not experimental. It is a mature protocol previously validated in adult populations, now demonstrated in a pediatric context.[10,16] The two presented cases were selected not as a typical case series, but rather to highlight the expanded utility and unique advantages of this protocol in children. Our analysis of radiation dose reduction is an original contribution that extends the utility of IV-DSA beyond workflow feasibility—quantifying its benefit through reproducible dose modeling.

The IV-DSA protocol also streamlines intraoperative workflow across surgical and radiological teams. Because it does not require real-time catheter control by an interventional radiologist, the surgical team can operate with greater autonomy and less operative time. In Case 2, IV-DSA-guided resection of a ruptured AVM cost only 6.5 hours while IA-DSA-guided surgery in Case 3 took 8 hours. This is particularly beneficial in pediatric centers with limited neurointerventional coverage. Reduced need for radiology personnel during navigation lowers coordination barriers, allows faster transitions between imaging and resection phases, and shortens anesthesia time—a critical advantage in pediatrics.

Role of i-Flow Timing and AR Navigation

Optimized imaging quality in our protocol was achieved through iFlow-based test rounds and delay time estimation. Unlike conventional CTA, which relies on aortic arch triggering or bolus tracking, iFlow enables real-time monitoring of intracranial vessel opacification, thus minimizing timing errors related to anatomical or cardiac variability. This benefit is particularly valuable in pediatric patients, who may exhibit non-standard hemodynamics. Our use of a 4 frames/s acquisition rate further limited unnecessary exposure while maintaining diagnostic quality.

Augmented reality (AR) guidance enhanced intraoperative orientation by projecting color-coded 3D vascular reconstructions directly onto the surgical field. This integration improved spatial perception and

reduced the cognitive load of switching between monitors and the microscope.[29] In unruptured AVMs, post-dural DSA allowed for accurate overlay alignment. In ruptured cases with brain edema and cortical shift (e.g., Case 2, 3), manual adjustments of the AR overlay ensured persistent accuracy. Compared to preoperative MDCT angiography-based navigation, which lacks adaptability to intraoperative deformation, our AR-enhanced approach preserved real-time anatomical relevance.

In Case 2, IV-DSA performed before dural opening allowed adequate visualization despite severe cerebral edema. Although AR projection required manual adjustment due to cortical shift, intraoperative anatomical feedback confirmed alignment accuracy. Notably, IV-DSA provided sufficient spatial data for determining safe dissection planes without the need for repeat IA injections. This further illustrates the feasibility of IV-DSA navigation even in dynamically changing operative fields, where IA-DSA would require time-consuming repositioning and catheter manipulation.

Limitations and Future Directions

Radiation dosimetry may vary across imaging platforms due to differences in manufacturer settings, system generations, and acquisition protocols. While our estimates were based on measured DAP values and established conversion factors, some variability in effective dose is inevitable. Additionally, current findings reflect early-phase clinical experience; broader validation in diverse pediatric cohorts will be essential to confirm consistency in imaging quality, radiation sparing, and surgical outcomes over time.

The IV-DSA AR protocol holds potential for broader application beyond AVMs, including dural sinus malformations, vein of Galen anomalies, and pediatric brain tumors with vascular involvement. Future investigations may incorporate real-time 4D flow mapping, AR drift correction, and artificial intelligence-driven vessel segmentation to further enhance intraoperative navigation. Multi-center studies will be necessary to assess reproducibility across platforms and teams, and to establish standardized pediatric IV-DSA guidelines.

In conclusion, IV-DSA–based AR guidance provides a safe, adaptable, and radiation-efficient imaging strategy for pediatric neurovascular surgery. As clinical experience expands, this protocol may serve as a foundation for more personalized, lower-risk, and workflow-integrated surgical planning in children. Its adaptability, safety profile, and imaging quality suggest potential for broader integration into pediatric neurovascular practice.

CONCLUSION

This study demonstrates the feasibility and clinical value of a standardized IV-DSA protocol integrated with AR-guided navigation in pediatric brain AVM surgery. By quantifying radiation exposure across multiple imaging modalities and demonstrating protocol adaptability to pediatric physiology, we provide evidence supporting IV-DSA as a safer, less invasive, and workflow-efficient alternative to conventional angiographic methods. Our dosimetric modeling, technical workflow, and intraoperative outcomes

highlight the potential for broader adoption of this technique beyond AVMs. As pediatric neurovascular surgery increasingly demands individualized, low-risk imaging strategies, the IV-DSA protocol offers a reproducible and scalable solution grounded in both imaging science and surgical practicality.

Funding and disclosures

This study was supported by the National Chung Hsing University, Chung Shan Medical University, Taiwan National Science and Technology Council (NSTC 113-2320-B-005-006), and Taichung Veterans General Hospital (Grant No. TCVGH-1134903B, TCVGH-CTUST1147702). Central Taiwan University of Science and Technology, Taiwan (114-OA080 TCVGH-CTUST1147702). The authors have no competing interests to declare.

Declarations

Acknowledgements

The authors are grateful to the National Chung Hsing University, Chung Shan Medical University, and Taichung Veterans General Hospital for providing administrative, technical, and funding support.

Funding and disclosures

This study was supported by the National Chung Hsing University, Chung Shan Medical University, Taiwan National Science and Technology Council (NSTC 113-2320-B-005-006), and Taichung Veterans General Hospital (Grant No. TCVGH-1134903B, TCVGH-CTUST1147702). Central Taiwan University of Science and Technology, Taiwan (114-OA080 TCVGH-CTUST1147702). The authors have no competing interests to declare.

Ethics approval

This study was approved by the Ethics Review Committee of Taichung Veterans General Hospital, Taichung, Taiwan (IRB no: CE17182A).

Patient consent for publication

Informed consent was obtained from the patients' parents.

Data availability statement

The datasets used in this study are available from the Ministry of Health and Welfare Taiwan, on reasonable request.

Funding and disclosures

This study was supported by the National Chung Hsing University, Chung Shan Medical University, Taiwan National Science and Technology Council (NSTC 113-2320-B-005-006), and Taichung Veterans General Hospital (Grant No. TCVGH-1134903B, TCVGH-CTUST1147702). Central Taiwan University of Science and Technology, Taiwan (114-OA080 TCVGH-CTUST1147702). The authors have no competing interests to declare.

Ethics approval

This study was approved by the Ethics Review Committee of Taichung Veterans General Hospital, Taichung, Taiwan (IRB no: CE17182A). The research was conducted in accordance with the Declaration of Helsinki. Informed consent was obtained from the legal guardians of all pediatric participants for their participation in this study and for the publication of the clinical findings.

Author Contributions

C.W.H. and C.C.C. contributed to the study conception and design. Material preparation, data collection, and analysis were performed by C.W.H. and K.C.C.. The first draft of the manuscript was written by C.W.H. and C.C.C., and all authors (P.Y.T., C.H.L., B.S.L., Y.S.T., S.F.Y.) commented on previous versions of the manuscript. All authors read and approved the final manuscript.

References

1. Nikolaev SI, Vetiska S, Bonilla X, et al. Somatic activating KRAS mutations in arteriovenous malformations of the brain. N Engl J Med. 2018;378(3):250–61. 10.1056/nejmoa1709449.
2. McDonald JS, McDonald RJ, Comin J, et al. Frequency of acute kidney injury following intravenous contrast medium administration: a systematic review and meta-analysis. Radiology. 2013;267(1):119–28. 10.1148/radiol.12121460.
3. Ravindra VM, Bollo RJ, Eli IM, et al. A study of pediatric cerebral arteriovenous malformations: clinical presentation, radiological features, and long-term functional and educational outcomes with predictors of sustained neurological deficits. J Neurosurg Pediatr. 2019;24(1):1–8. 10.3171/2019.2.PEDS18731.
4. El-Ghanem M, Kass-Hout T, Kass-Hout O, et al. Arteriovenous malformations in the pediatric population: review of the existing literature. Interv Neurol. 2016;5(3–4):218–25. 10.1159/000447605.
5. Zheng T, Wang Q-J, Liu Y-Q, et al. Clinical features and endovascular treatment of intracranial arteriovenous malformations in pediatric patients. Childs Nerv Syst. 2014;30(4):647–53. 10.1007/s00381-013-2277-3.
6. Di Rocco C, Tamburrini G, Rollo M. Cerebral arteriovenous malformations in children. Acta Neurochir (Wien). 2000;142(2):145–56. 10.1007/s007010050017. discussion 156.
7. Derdeyn CP, Zipfel GJ, Albuquerque FC, et al. Management of brain arteriovenous malformations: a scientific statement for healthcare professionals from the American Heart Association/American

Stroke Association. Stroke. 2017;48(8):e200–24. 10.1161/STR.0000000000000134.

8. Daley SF, Avva U. Pediatric dehydration. StatPearls. Treasure Island, FL: StatPearls Publishing; 2024.
9. Guyther J, Wiltjer R. Pediatric trauma. Emerg Med Clin North Am. 2023;41(1):205–22. 10.1016/j.emc.2022.09.002.
10. Huang C-W, Lee C-H, Chung K-C, Tsuei Y-S. Feasibility and workflow analysis of IV-DSA-based augmented reality-guided brain arteriovenous malformation resection in a hybrid operating room: I-Flow tailored method [published online September 28, 2023]. J Neurointerv Surg. 10.1136/jnis-2023-020797
11. Nien Y-N. Evaluation of effective dose and conversion factors for liver and brain interventional fluoroscopy [Master's thesis, Chung Shan Medical University]. Airiti Library, 2019.
12. Manninen A-L, Isokangas J-M, Karttunen A, Siniluoto T, Nieminen MT. A comparison of radiation exposure between diagnostic CTA and DSA examinations of cerebral and cervicocerebral vessels. AJNR Am J Neuroradiol. 2012;33(11):2038–42. 10.3174/ajnr.A3123.
13. Struffert T, Hauer M, Banckwitz R, Köhler C, Royalty K, Doerfler A. Effective dose to patient measurements in flat-detector and multislice computed tomography: a comparison of applications in neuroradiology. Eur Radiol. 2014;24(6):1257–65. 10.1007/s00330-014-3136-7.
14. Mnyusiwalla A, Aviv RI, Symons SP. Radiation dose from multidetector row CT imaging for acute stroke. Neuroradiology. 2009;51(10):635–40. 10.1007/s00234-009-0543-6.
15. McParland BJ. A study of patient radiation doses in interventional radiological procedures. Br J Radiol. 1998;71(842):175–85. 10.1259/bjr.71.842.9579182.
16. Ozaydin B, Dawkins DW, Armstrong SA, Aagaard-Kienitz B, Baskaya MK. Intraoperative application of a new-generation 3D IV-DSA technology in resection of a hemorrhagic cerebellar AVM. Neurosurg Focus Video. 2021;4(1):V10. 10.3171/2020.10.FOCVID2086.
17. Thust SC, Chong WKK, Gunny R, et al. Paediatric cerebrovascular CT angiography-towards better image quality. Quant Imaging Med Surg. 2014;4(6):469–74. 10.3978/j.issn.2223-4292.2014.10.09.
18. PDQ Pediatric Treatment Editorial Board. Late effects of treatment for childhood cancer (PDQ®): Health professional version. In: PDQ Cancer Information Summaries [Internet]. Bethesda, MD: National Cancer Institute. 2024. Available at https://www.ncbi.nlm.nih.gov/books/NBK65832/figure/CDR0000343584__2719/
19. Charles MW. 103: Recommendations of the ICRP. ICRP Publication; 2008.
20. Fuss M, Poljanc K, Hug EB. Full Scale IQ (FSIQ) changes in children treated with whole brain and partial brain irradiation. A review and analysis. Strahlenther Onkol. 2000;176(12):573–81. 10.1007/pl00002327.
21. Gaballah M, Storm PB, Rabinowitz D, et al. Intraoperative cerebral angiography in arteriovenous malformation resection in children: a single institutional experience. J Neurosurg Pediatr. 2014;13(2):222–8. 10.3171/2013.10.PEDS13291.

22. Ghosh S, Levy ML, Stanley P, Nelson M, Giannotta SL, McComb JG. Intraoperative angiography in the management of pediatric vascular disorders. Pediatr Neurosurg. 1999;30(1):16–22. 10.1159/000028754.
23. Ellis MJ, Kulkarni AV, Drake JM, Rutka JT, Armstrong D, Dirks PB. Intraoperative angiography during microsurgical removal of arteriovenous malformations in children. J Neurosurg Pediatr. 2010;6(5):435–43. 10.3171/2010.8.PEDS10134.
24. Klopfenstein JD, Spetzler RF, Kim LJ, et al. Comparison of routine and selective use of intraoperative angiography during aneurysm surgery: a prospective assessment. J Neurosurg. 2004;100(2):230–5. 10.3171/jns.2004.100.2.0230.
25. Ge B, Wei Y. Comparison of transfemoral cerebral angiography and transradial cerebral angiography following a shift in practice during four years at a single center in China. Med Sci Monit. 2020;26:e921631. 10.12659/MSM.921631.
26. Alehaideb A, Ha W, Bickford S, et al. Can children be considered for transradial interventions? prospective study of sonographic radial artery diameters. Circ Cardiovasc Interv. 2020;13(7):e009251. 10.1161/CIRCINTERVENTIONS.120.009251.
27. Irving C, Zaman A, Kirk R. Transradial coronary angiography in children and adolescents. Pediatr Cardiol. 2009;30(8):1089–93. 10.1007/s00246-009-9502-6.
28. Lee SB, Cho YJ, Kim S-H, Lee S, Choi YH, Cheon J-E. Transradial cerebral angiography: is it feasible and safe for children? Cardiovasc Interv Radiol. 2022;45(4):504–9. 10.1007/s00270-022-03070-w.
29. Li C-R, Shen C-C, Yang M-Y, Tsuei Y-S, Lee C-H. Intraoperative augmented reality in microsurgery for intracranial arteriovenous malformation: a case report and literature review. Brain Sci. 2023;13(4):653. 10.3390/brainsci13040653.

Figures

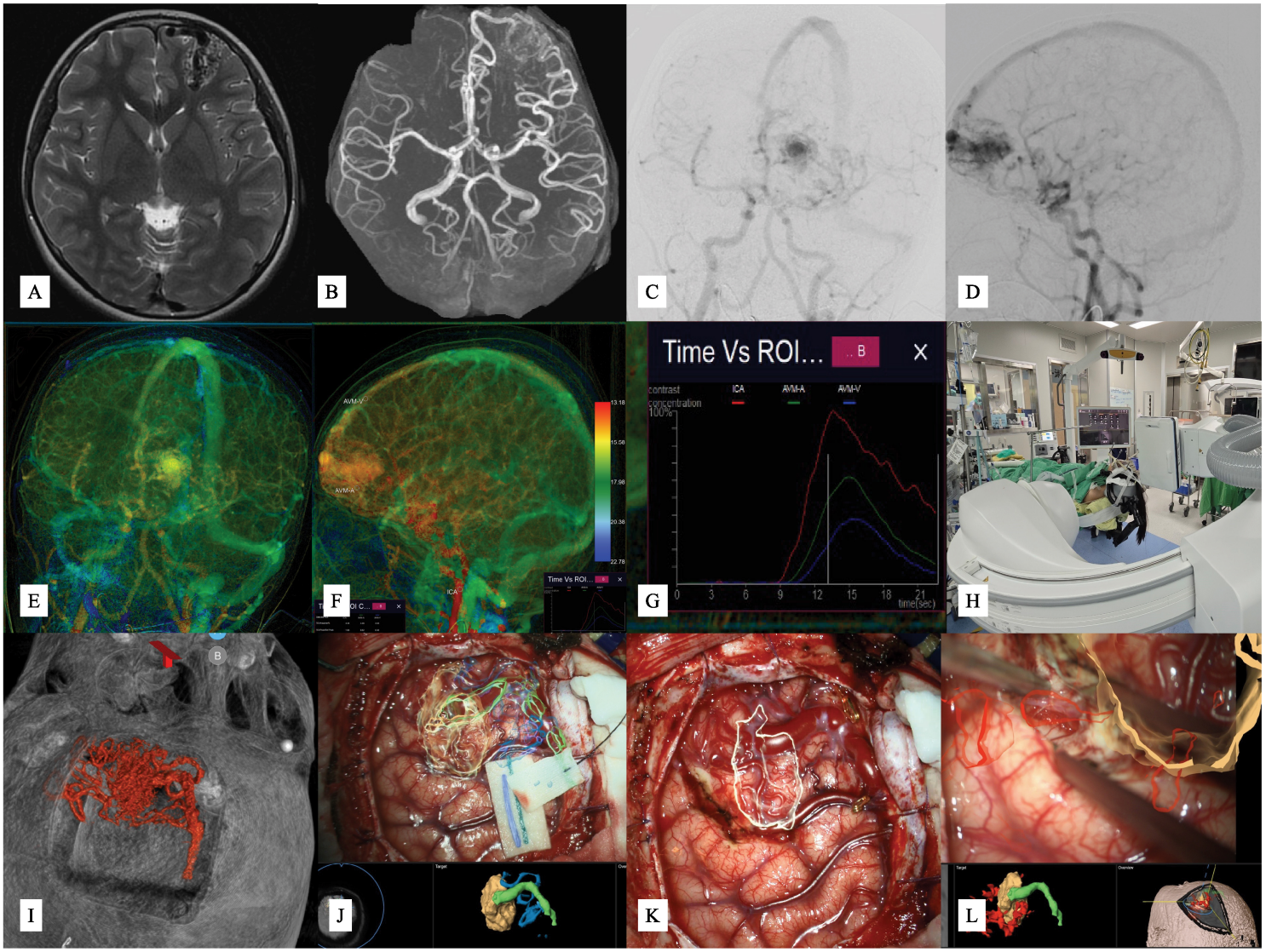


Figure 1

A school-aged child (Case 1) was diagnosed with an unruptured left frontal arteriovenous malformation (AVM; Spetzler–Martin grade I) (A, B). Intravenous digital subtraction angiography (C, D) revealed two main feeding arteries originating from the left anterior cerebral artery, several minor feeding arteries from the left middle cerebral artery, and one superficial drainage vein. We used the iFlow system (ARTIS icono biplane angiography system; Siemens Healthineers, Erlangen, Germany) (E–H) to predict the triggering time by tracking the opacification of the intracranial vessels and nidus. We also employed 3D digital subtraction angiography (DSA), which outlined the AVM lesion and the location in the skull (I). We labeled the contours of the nidus (yellow), superficial drainage vein (green), superficial feeding arteries (blue), and deep feeding arteries (red) below the nidus. The AR image was precisely projected onto the brain surface where brain AVM (bAVM) was located (J, K). When we began to resect the caudal site of bAVM, augmented reality navigation guided us on the nidus margin and the direction of feeding arteries below (L).

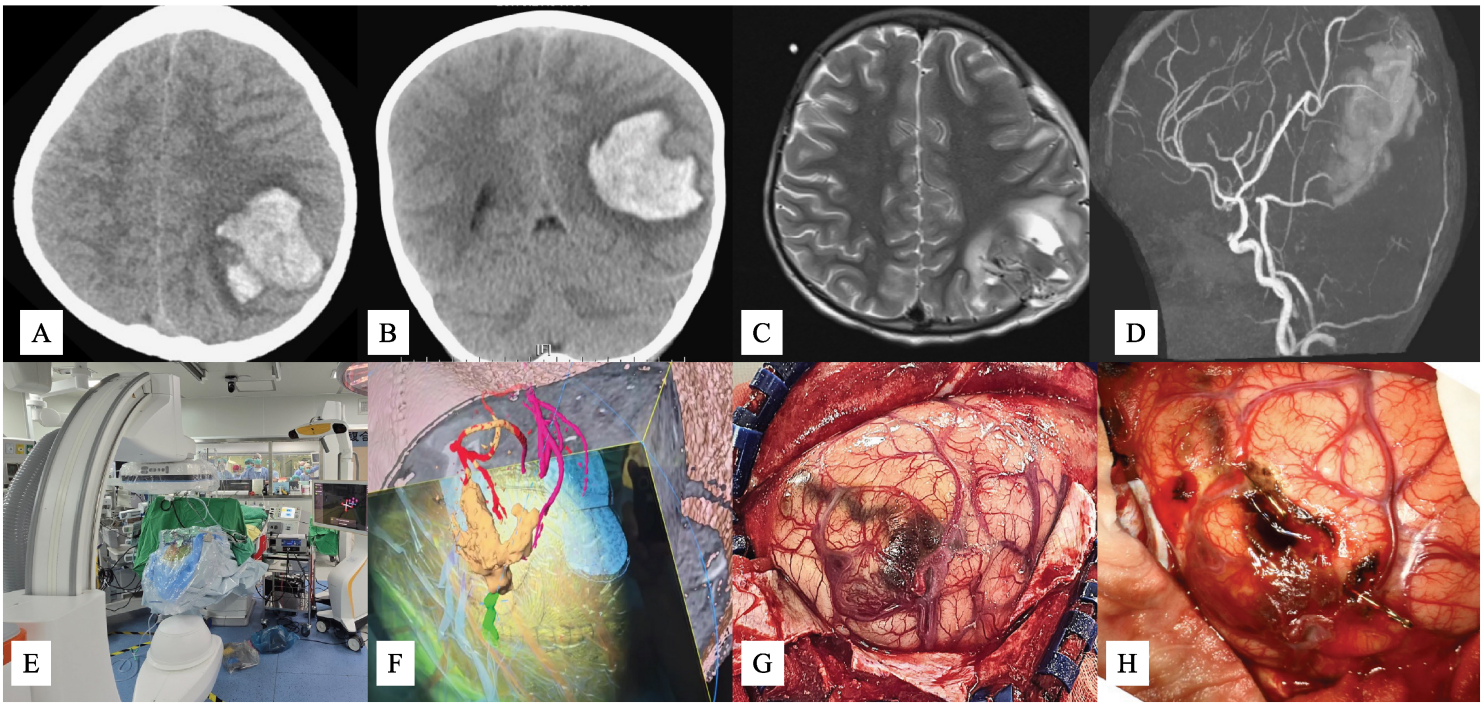


Figure 2

A preschool-aged child (Case 2) presented with a ruptured left parietal–occipital arteriovenous malformation with altered consciousness and signs of increased intracranial pressure. Initial brain computed tomography revealed a left parietal–occipital intracerebral hemorrhage with a midline shift (A, B). Magnetic resonance angiography showed persistent brain swelling after decompressive craniectomy (C, D). bAVM resection was performed in a hybrid room equipped with an ARTIS icono biplane angiography system (E). We delineated the nidus (yellow), superficial drainage vein (green), and feeding arteries (pink and red) originating from the left middle cerebral artery and adjacent gyrus (light blue; F). Severe brain shift occurred after dural opening (G). After manual adjustment of the augmented reality projection, we regained a sense of direction and smoothly resected the bAVM as planned (H).

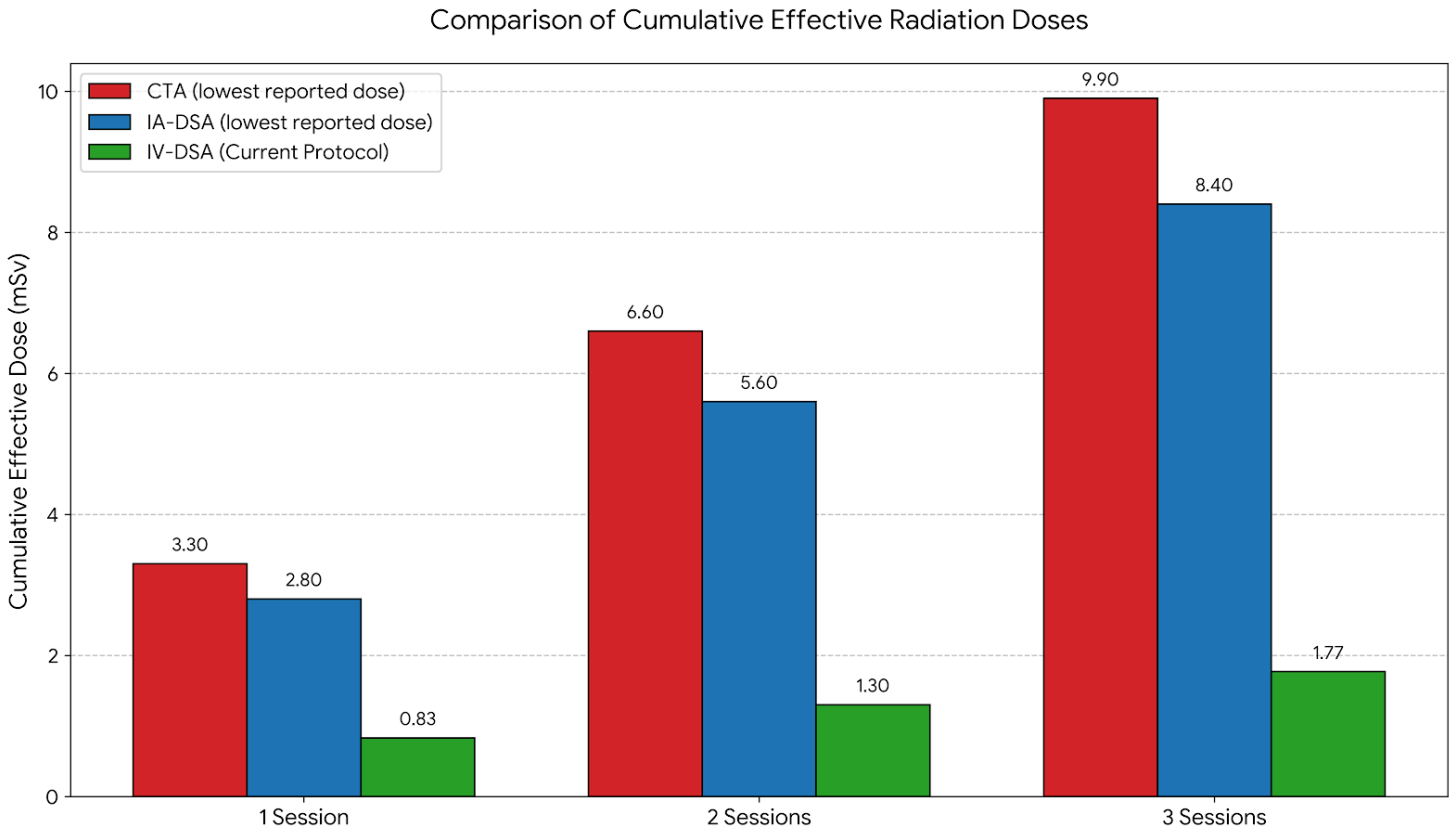


Figure 3

Comparison of cumulative effective radiation doses. Comparison of the cumulative effective doses (mSv) among intravenous digital subtraction angiography (IV-DSA), computed tomography angiography (CTA), and intra-arterial digital subtraction angiography (IA-DSA) across one, two, and three imaging sessions. The graph illustrates the substantial radiation-sparing advantage of the IV-DSA protocol compared to conventional modalities at every time point.